Identifying the possible ex-situ origin of the globular clusters of the Milky Way: a kinematic study

A. R. Shirazi, P. Khalaj, H. Haghi
arXiv:2310.04492

Edoardo Lagioia

SWIFAR Group Meeting - 10 November 2023

Galactic archaeology

Galactic archaeologists study the history of our galaxy using detailed observations of the Milky Way gas distribution and composition, star chemical enrichment and evolution, and the kinematic properties of different stellar groups

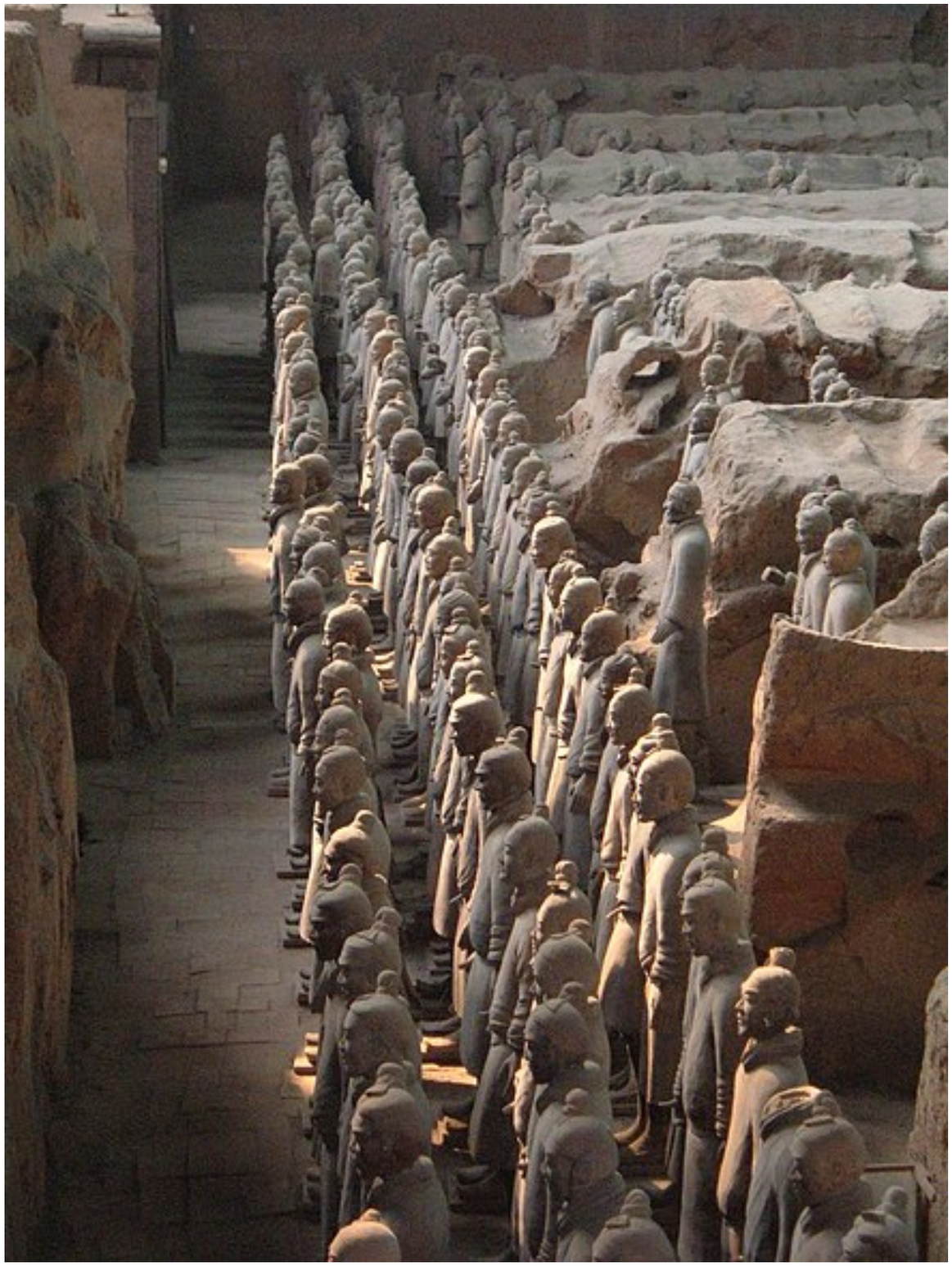

Terracotta Army of the Mausoleum of the First Qin Emperor

Searle & Zinn 1978

COMPOSITIONS OF HALO CLUSTERS AND THE FORMATION OF THE GALACTIC HALO

LEONARD SEARLE AND ROBERT ZINN
Hale Observatories, Carnegie Institution of Washington, California Institute of Technology
Received 1978 March 2; accepted 1978 April 21

ABSTRACT

A new method of abundance determination, based upon reddening-independent characteristics of low-resolution spectral scans, has been applied to 177 red giants in 19 globular clusters. Most of these clusters have galactocentric distances exceeding 8 kpc. We find that there is no radial abundance gradient in the cluster system of the outer halo. The distribution over abundance for these outer clusters appears to be independent of galactocentric distance and is nearly identical to that for halo subdwarfs in the solar neighborhood. This distribution is such that the density declines exponentially with increasing metal abundance. The clusters of the outer halo show a broad spread in the color distribution on the horizontal branch, and this property is uncorrelated with metal abundance. In contrast, more tightly bound clusters, in the same range of abundance, show very little dispersion in this property. These facts are all consistent with the hypothesis that the loosely bound clusters of the outer halo have a broader range of age than the more tightly bound clusters and originated in transient protogalactic fragments that continued to fall into dynamical equilibrium with the Galaxy for some time after the collapse of its central regions had been completed.

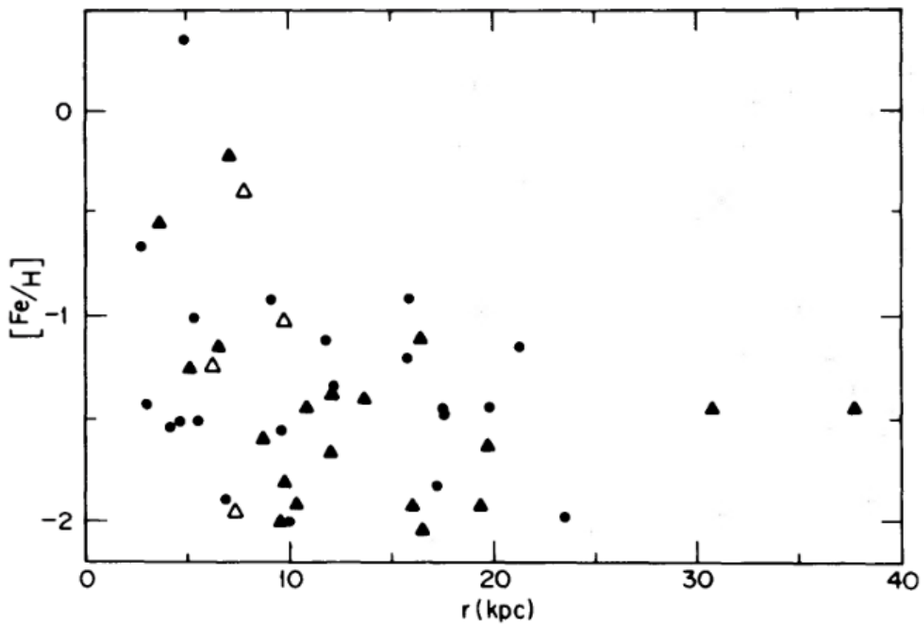

FIG. 9.—Abundances plotted against galactocentric distance for all clusters with tolerable estimates of both quantities. The solid triangles are the clusters studied in this paper. Open triangles are other clusters with first-rate abundance determinations. The circles represent clusters for which the abundance estimates were taken from Kukarkin (1974). Outside $r = 8$ kpc, the distribution over abundance does not change significantly with galactocentric distance.

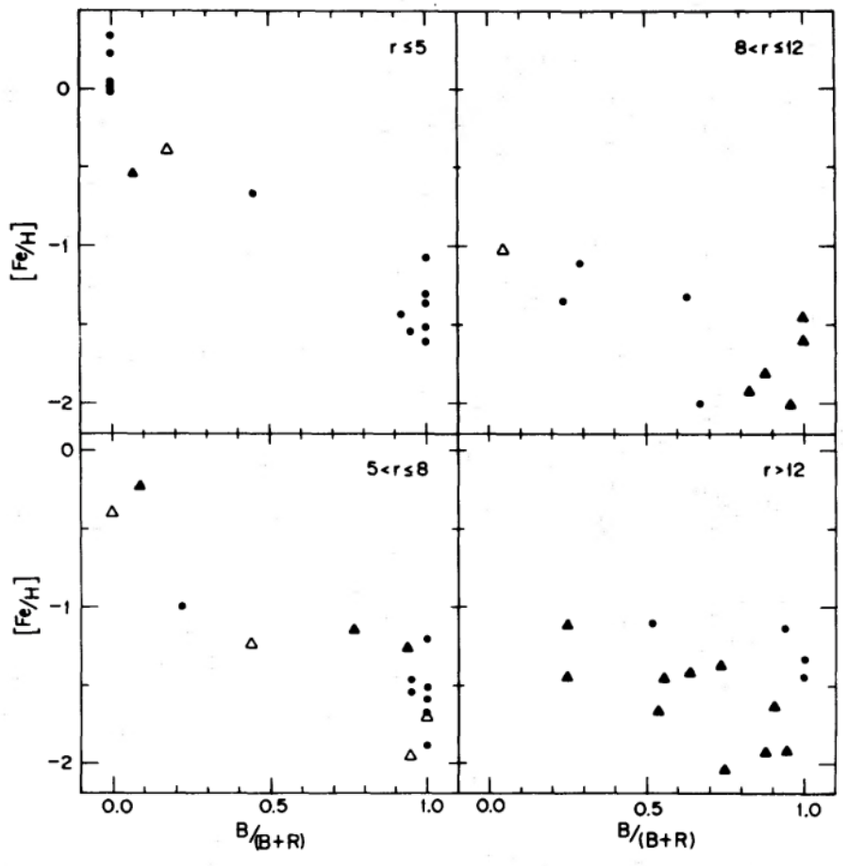

FIG. 10.—For all clusters with $r < 40$ kpc and for which color-magnitude diagrams exist, abundance is plotted against a parameter measuring the color distribution of the horizontal-branch stars. The four panels refer to clusters located in different intervals of galactocentric distance. The symbols are as in Fig. 9. The figure shows that, for clusters of the inner halo, the morphology of the color-magnitude (C-M) array depends on abundance, while for clusters in the outer halo there is a great diversity of c-m morphology at a given abundance.

Bellazzini+ 2002

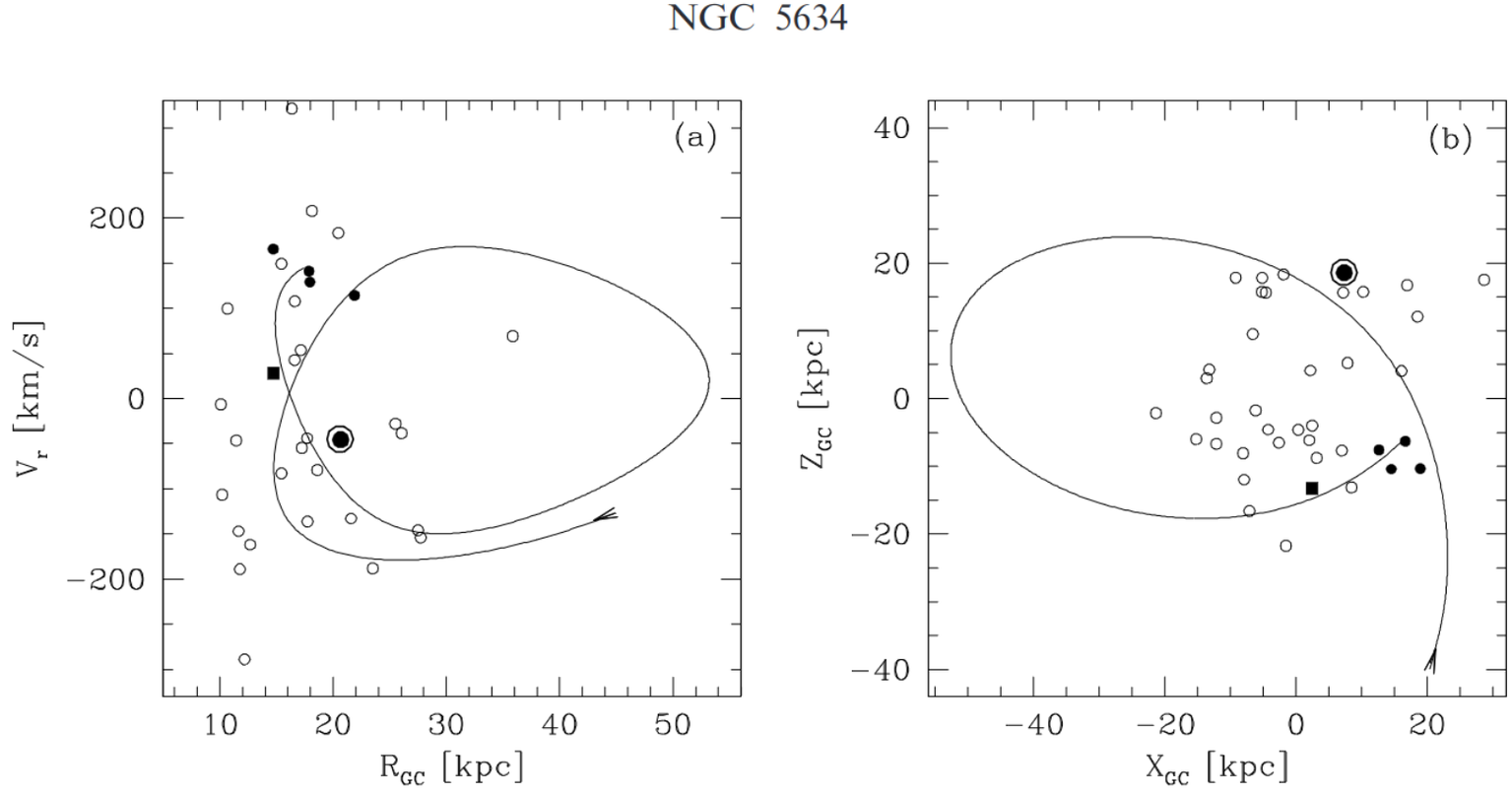

The globular clusters presently associated with the main body of the Sagittarius dSph, i.e., M54, Ter 8, Arp 2, and Ter 7, are plotted as small filled circles. The position of NGC 5634 is marked by a large filled circle.

Lambda CDM model

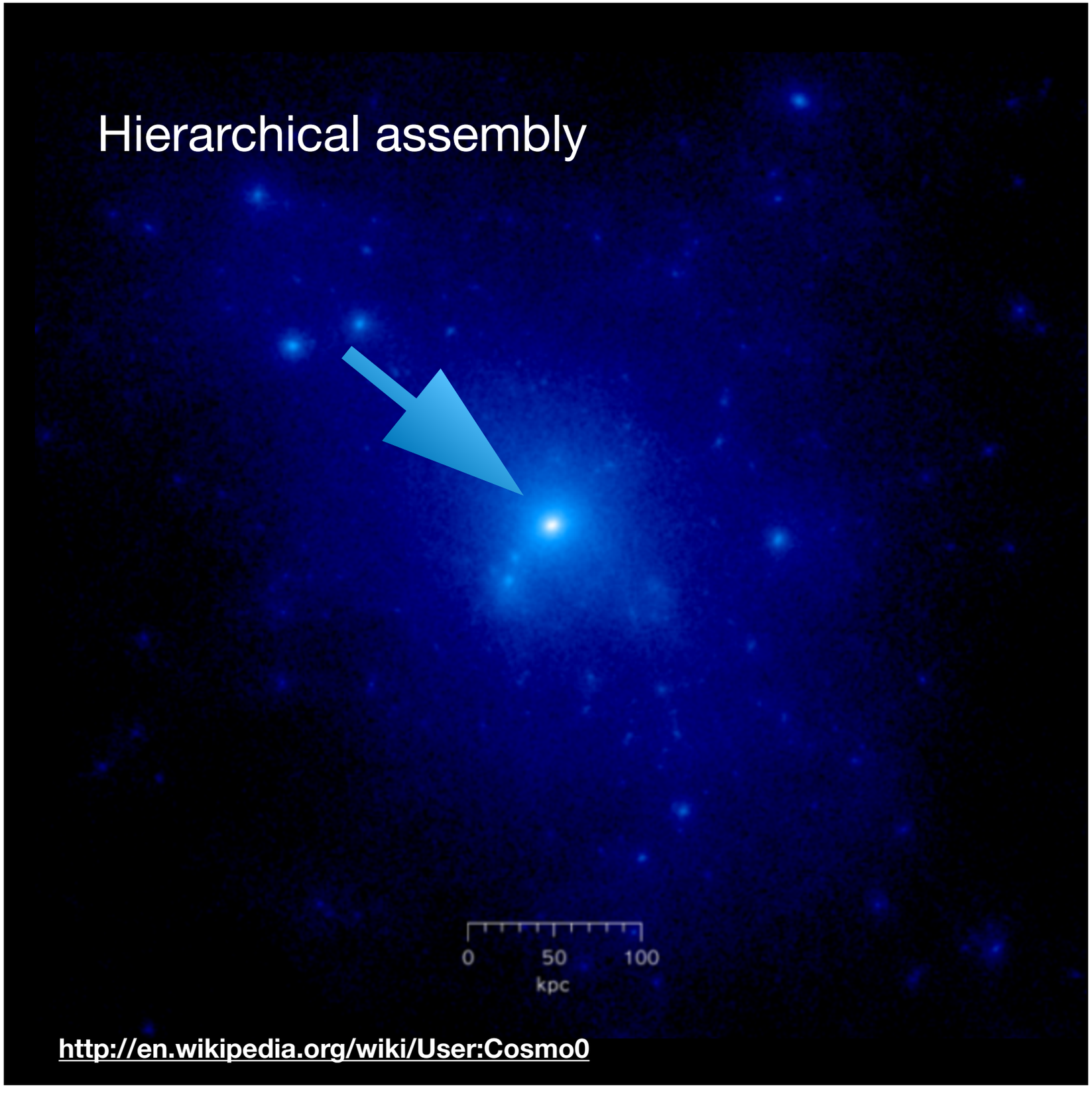

MW Stars

In situ

gas in the innermost regions of the Galaxy

Ex situ

progenitor dwarf satellite (merged) or still orbiting dwarf galaxy

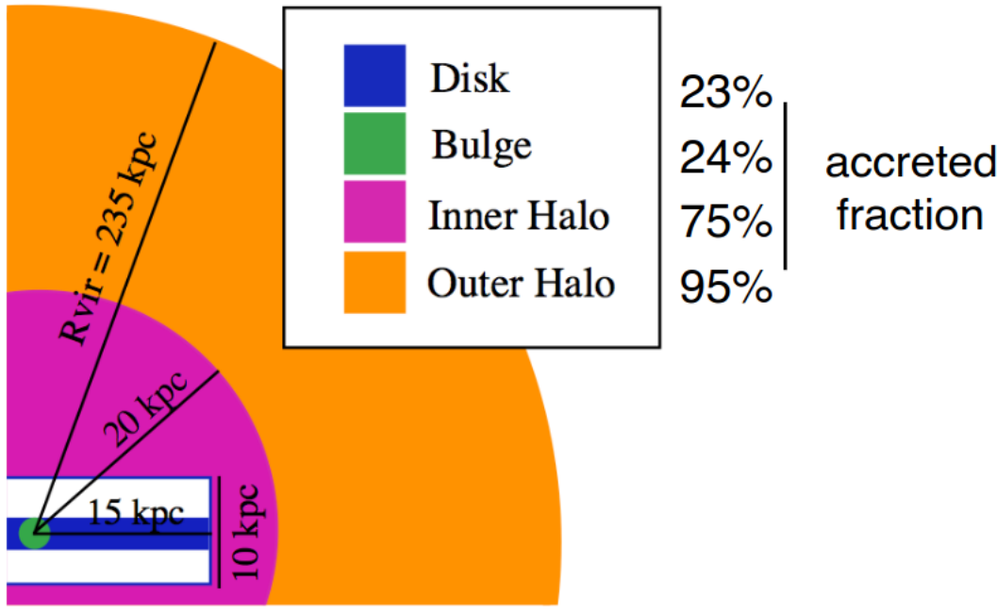

Pillepich, Madau & Mayer 2015

ERIS simulation

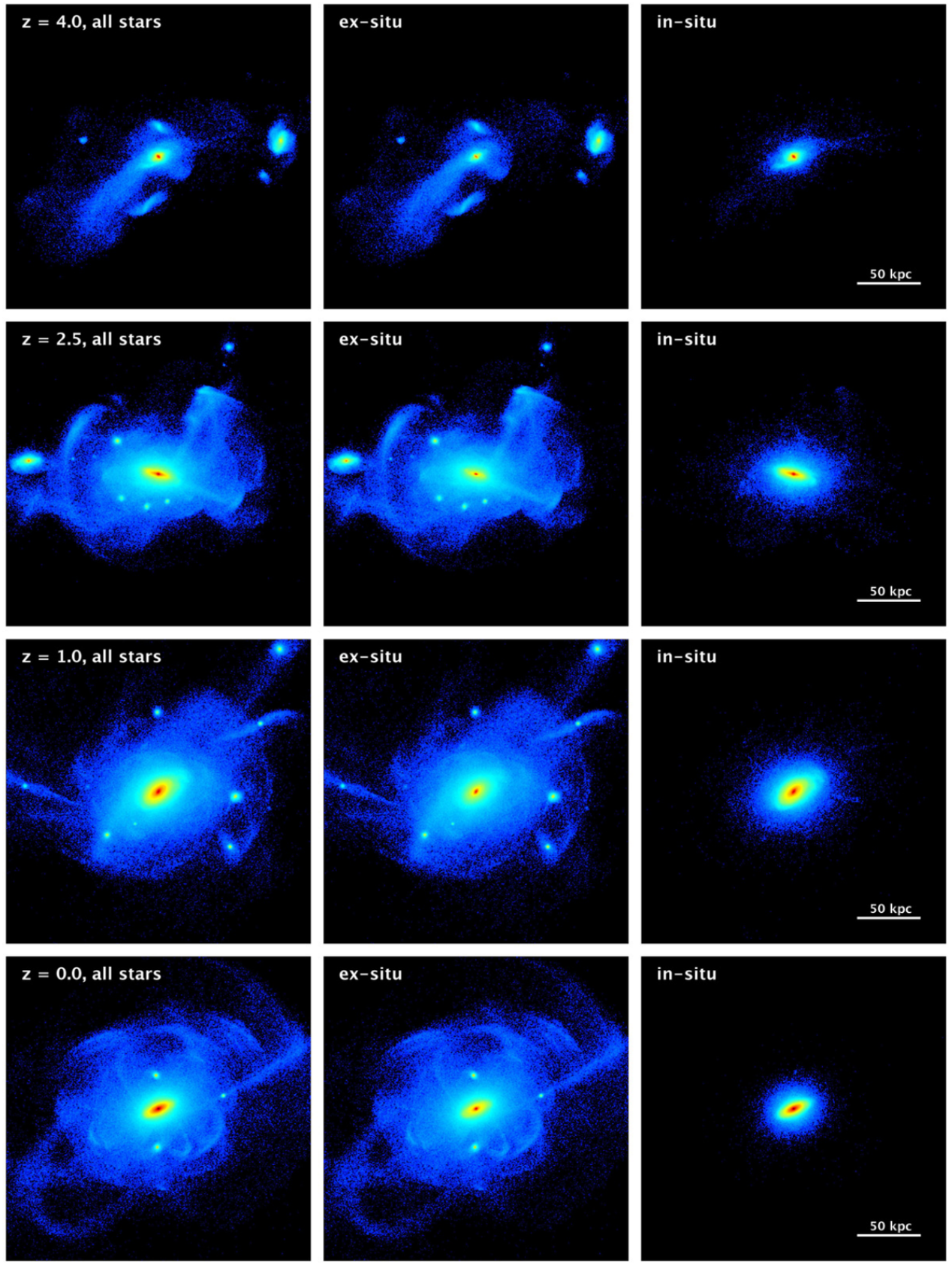

Figure 1. Random projection Eris's stellar density field in a (240 comoving kpc)^3 box, from $z \sim 4$ (top) to today (bottom). The middle and right columns show only stars formed ex-situ and in-situ, respectively. Surface mass densities range from 100 to 10^8 $M_\odot$ kpc^{-2}.

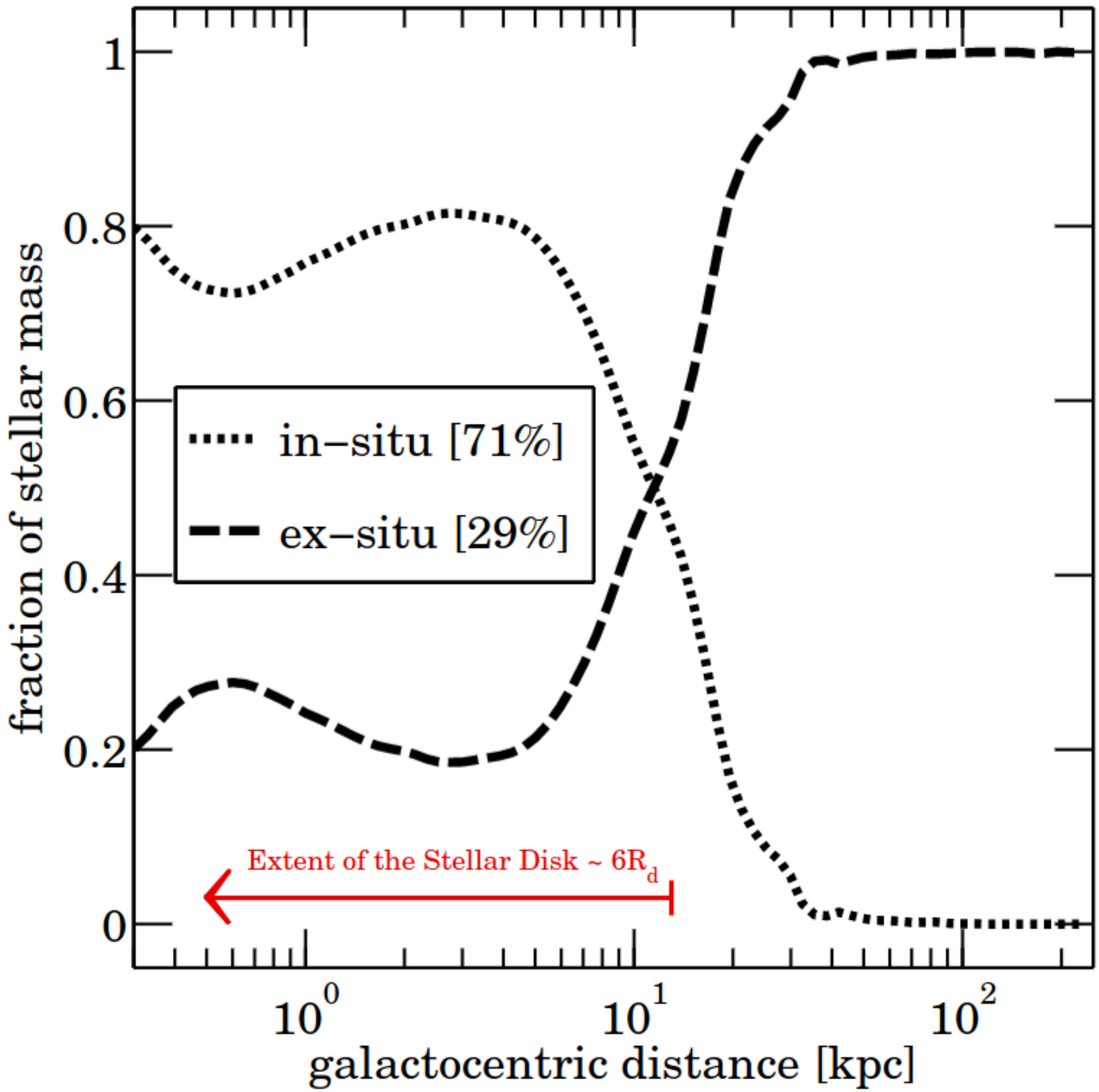

Pillepich, Madau & Mayer 2015

Sagittarius Stream - Ibata+ 1994

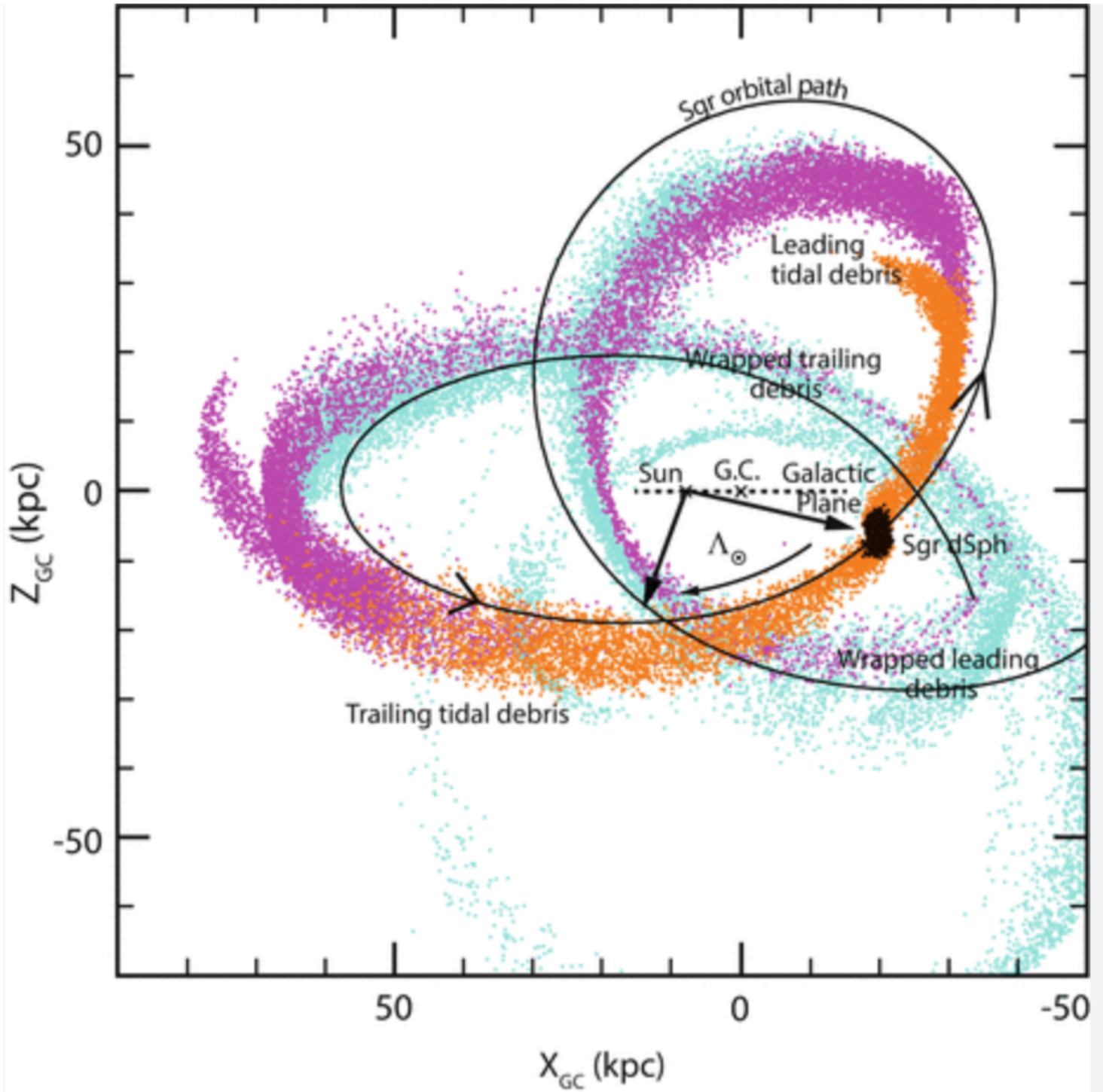

Law, D.R., Majewski, S.R. (2016). The Sagittarius Dwarf Tidal Stream(s). In: Newberg, H., Carlin, J. (eds) Tidal Streams in the Local Group and Beyond. Astrophysics and Space Science Library, vol 420. Springer

Geisler+ 1991

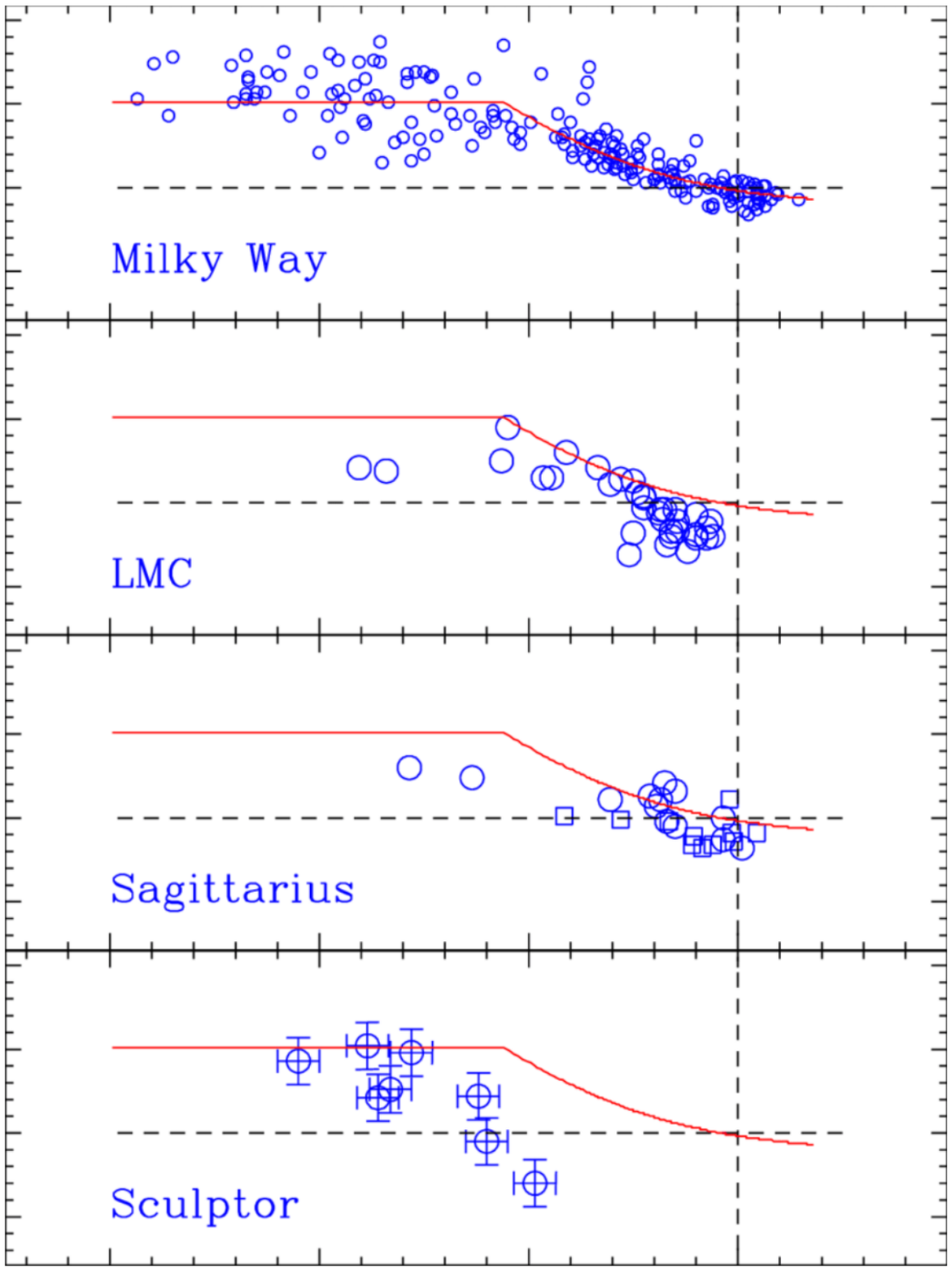

-[O/Fe] vs. [Fe/H] for samples of stars in 4 different galaxies. The solid curve is a model fit described in the text. O abundances in the extraGalactic samples are generally depleted with respect to their Galactic counterparts.

[alpha/Fe]

vs

[Fe/H]

Sbordone+ 2007

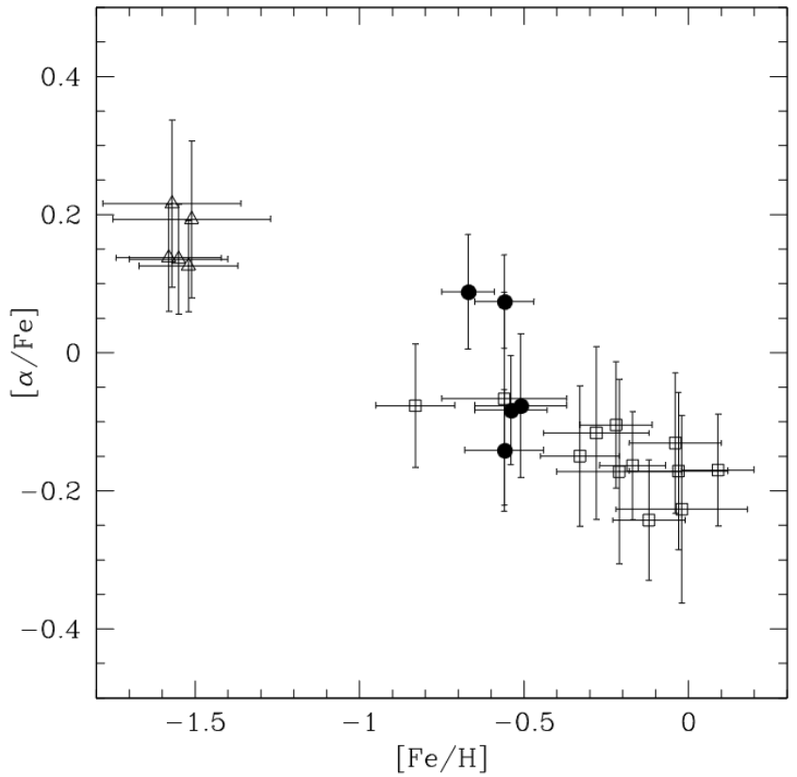

Fig. 4. [α/Fe] vs. [Fe/H] for the five stars of Terzan 7 (filled dots), the 12 stars in the Sgr dSph main body studied in Paper I (open squares), and the five stars in M 54 from Brown et al. (1999) (open triangles). α is defined as the mean of Mg, Si, and Ca.

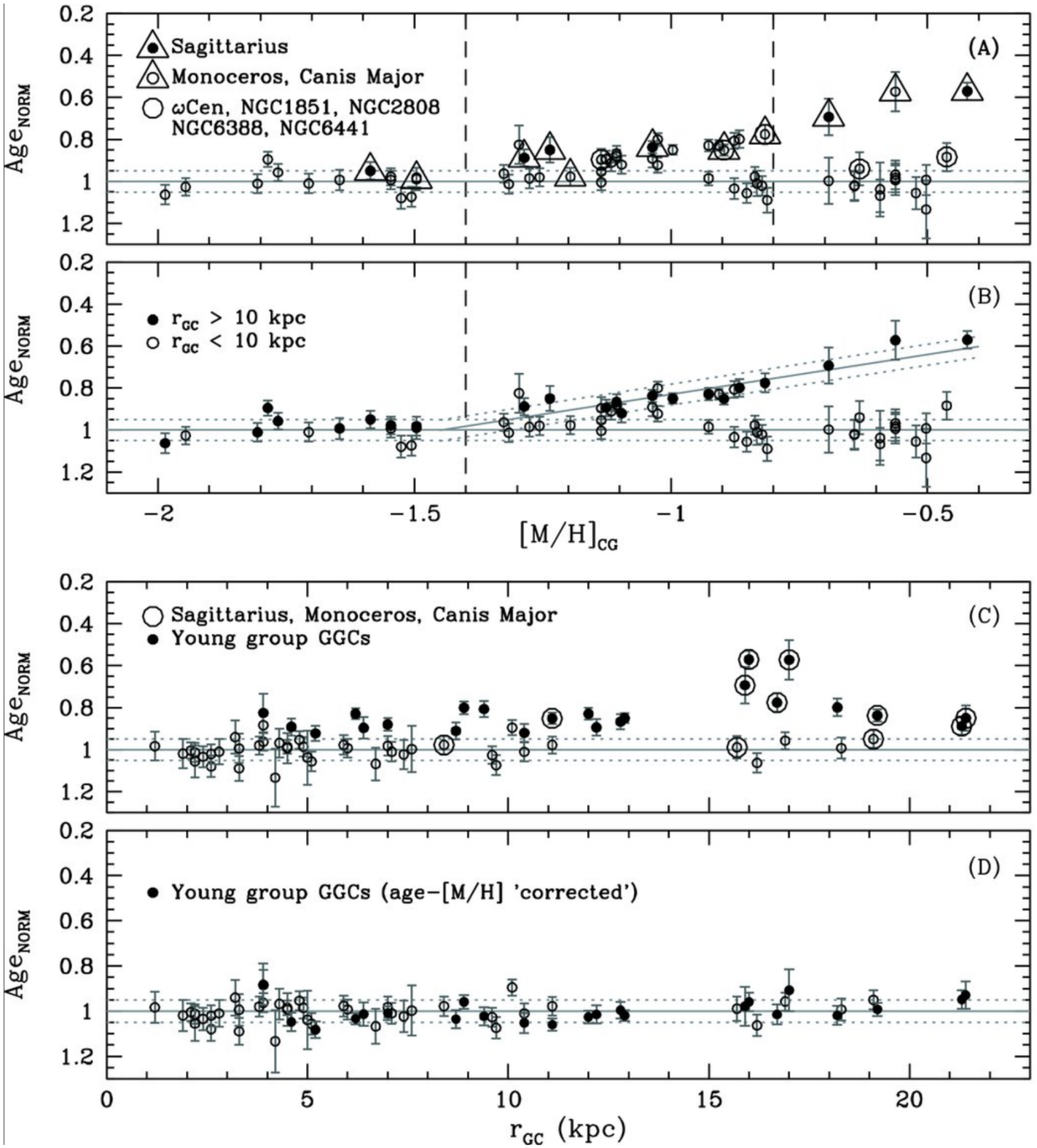

Marin-Franch+ 2009

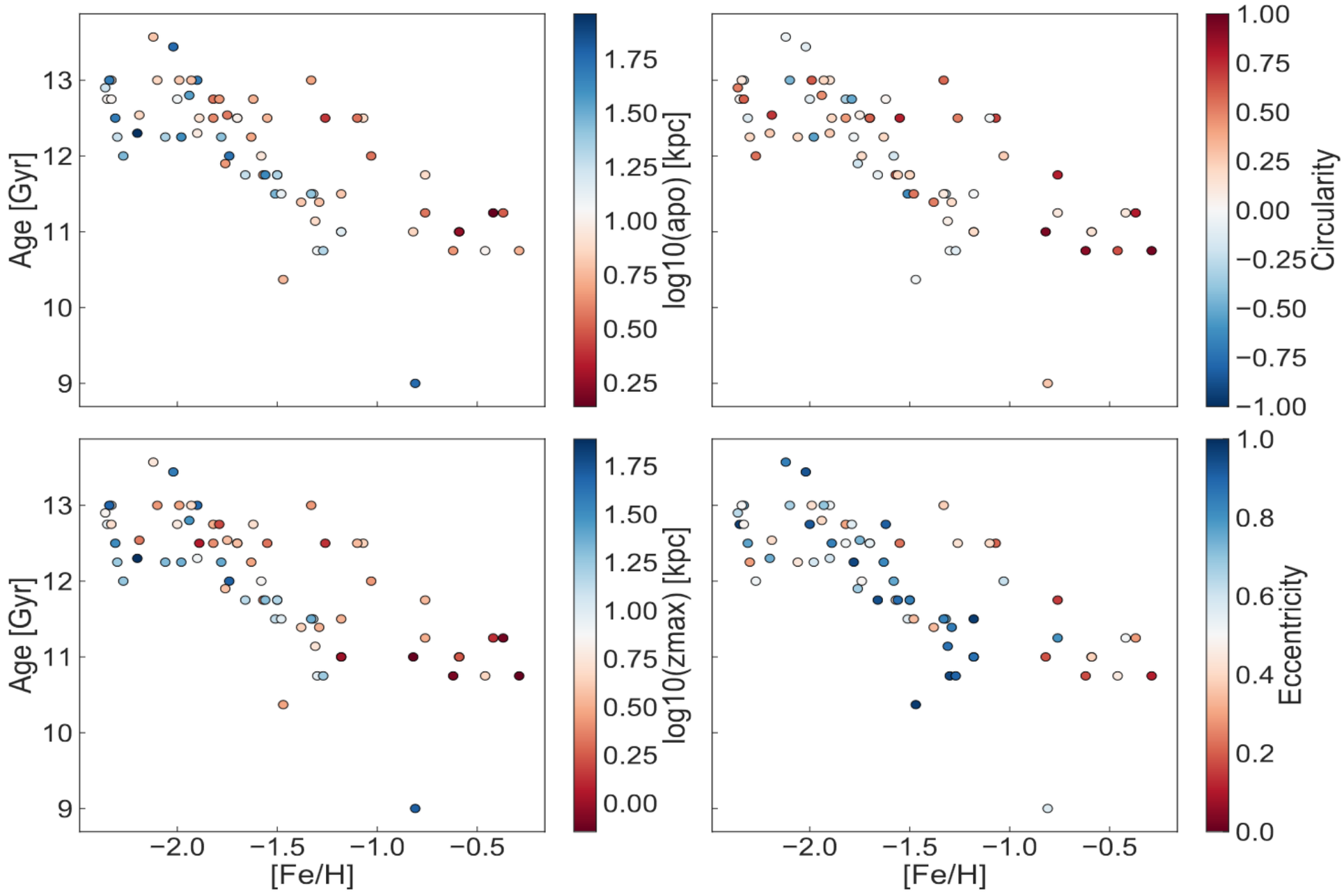

Massari+ 2019

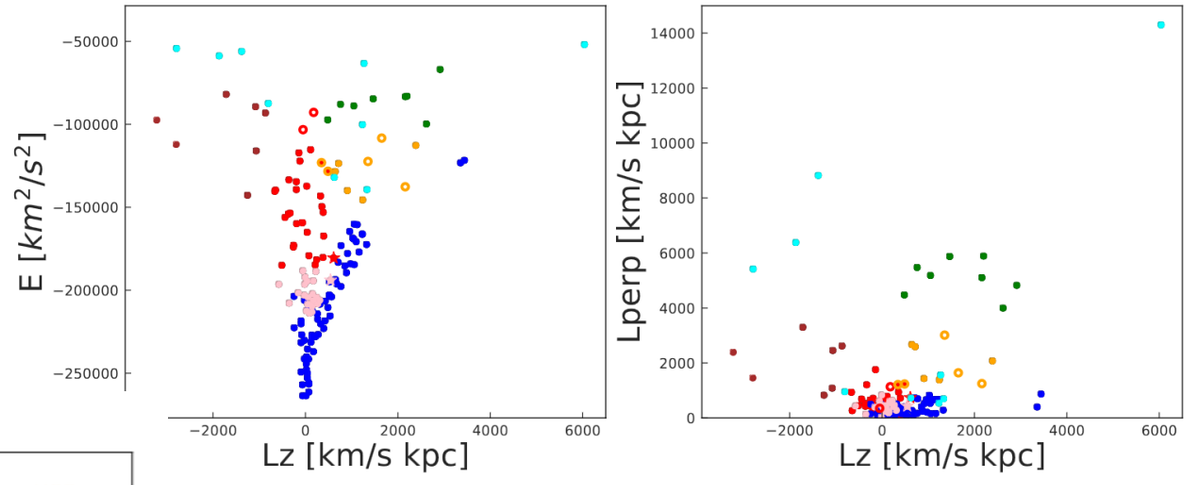

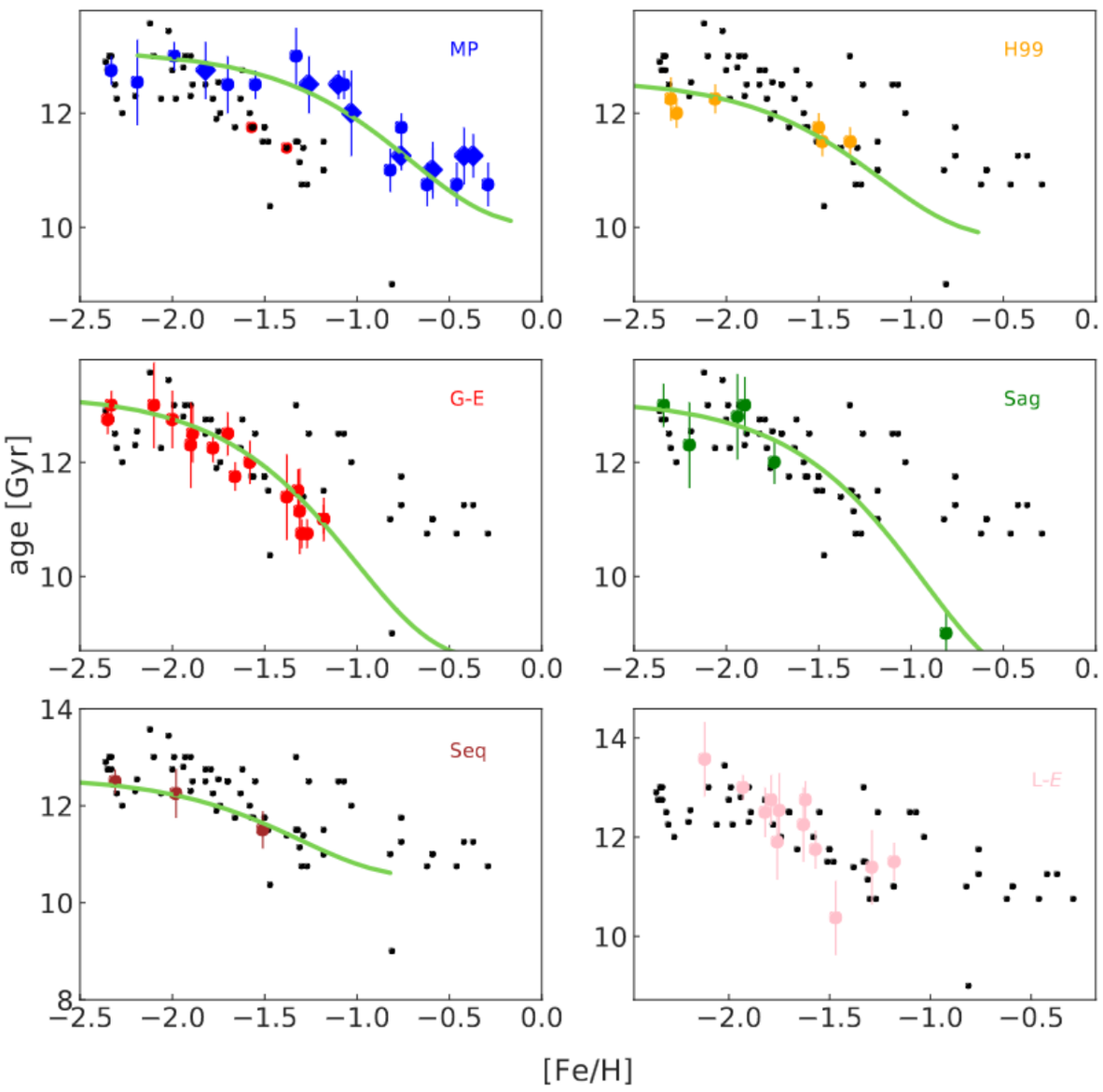

Massari+ 2019

Gaia - Enceladus collision

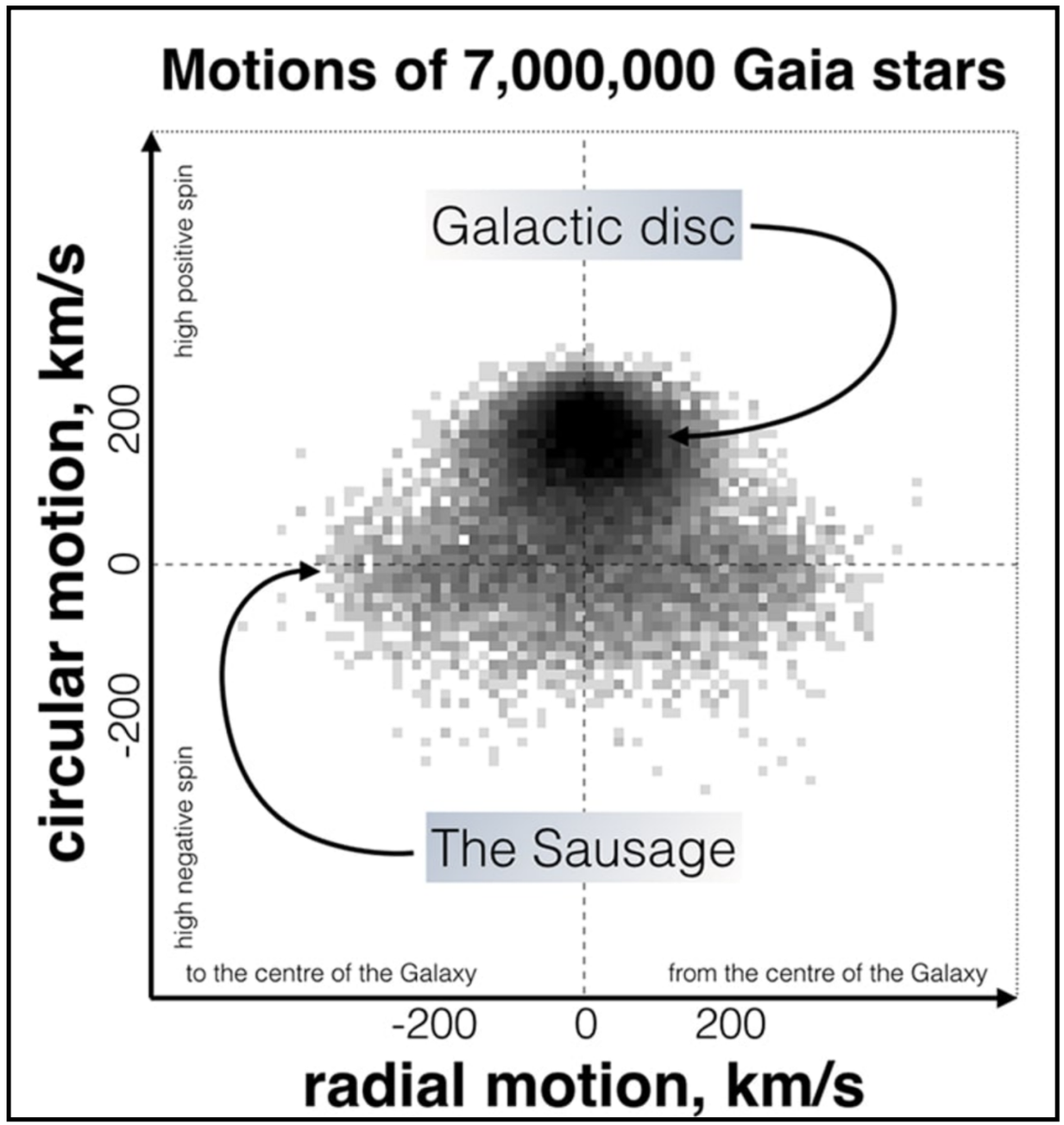

The name "Enceladus" refers to the mythological giant Enceladus, who was buried under Mount Etna and caused earthquake.

- based on Gaia DR2 data
- Kinematics of metal-rich halo stars
- Collision of a dwarf galaxy with 5 x 10^{10} M_{sun} at z ~ 3

Belukurov+ 2018

Myeong+ 2018

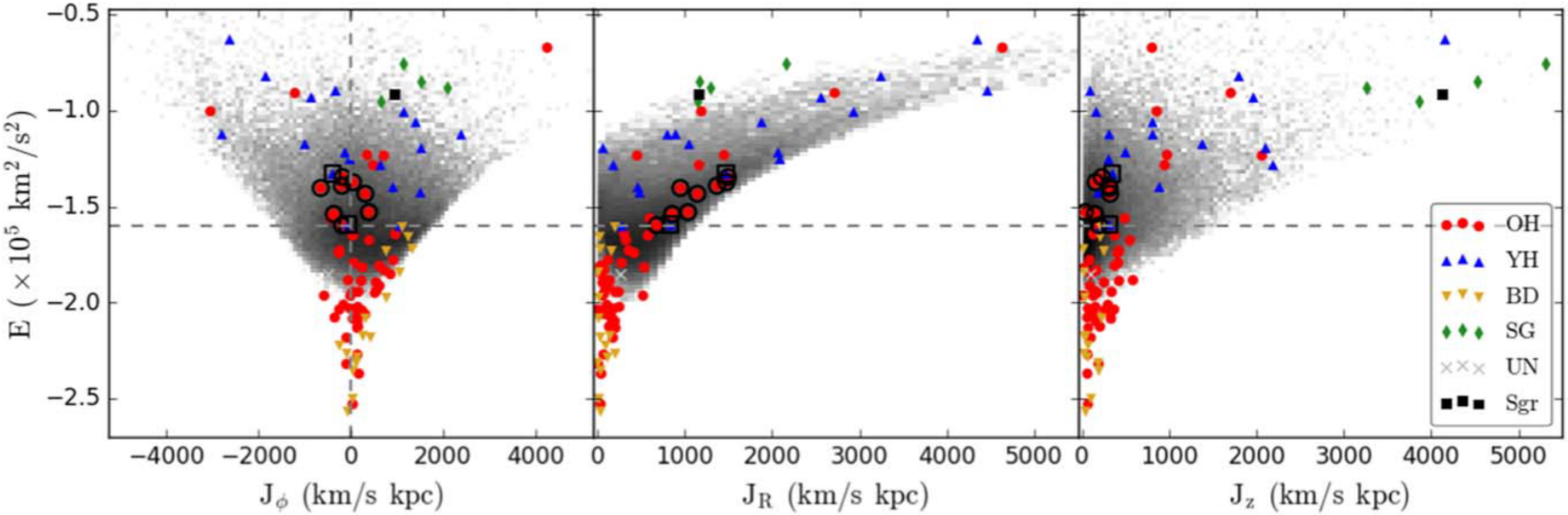

Figure 1. Distribution of GCs in energy-action space or (J_ϕ, E), (J_R, E), and (J_z, E) space. The grayscale background shows the halo MSTO stars from Myeong et al. (2018a) as a comparison. There are 75 GCs with *Gaia* DR2 proper motions and a further 16 with *Hubble Space Telescope* (*HST*) proper motions; 53 OHs (red circles), 17 YHs (blue triangles), 16 BDs (yellow triangles), and 4 Sgr GCs (SG; green diamonds) together with one of unknown classification (gray cross). Sgr is also marked as a black filled square. The vertical dashed line marks the division between prograde ($J_\phi > 0$) and retrograde ($J_\phi < 0$). The horizontal dashed line signifies the characteristic energy above which all of the YHs lie, and below which all of the BDs lie. The eight OH globular clusters, with symbols that are enclosed by black open circles, are grouped together in (J_ϕ, E) and (J_z, E), while in (J_R, E) they are stretched out close to the boundary of J_R at corresponding energy (as judged from the MSTOs). They are the Sausage GCs. The two YHs enclosed with black open squares form an extended selection that may also be related. They have horizontal branch morphology similar to OHs, and have similar actions.

8 GCs with E> E_{crit} belonging to the Gaia-Enceladus *Sausage*

This is a Digitized Sky Survey 2 image of the dwarf galaxy Fornax. Highlighted here are four globular clusters found in the galaxy called Fornax 1, 2, 3 and 5.

New observations of the four clusters — large balls of stars that orbit the centres of galaxies — show they are very similar to those found in our galaxy, the Milky Way. The finding is at odds with leading theories on how these clusters form — in these theories, globular clusters should be nestled among large quantities of old stars — and so the mystery of how these objects came to exist deepens.

Credit: ESO/Digitized Sky Survey 2

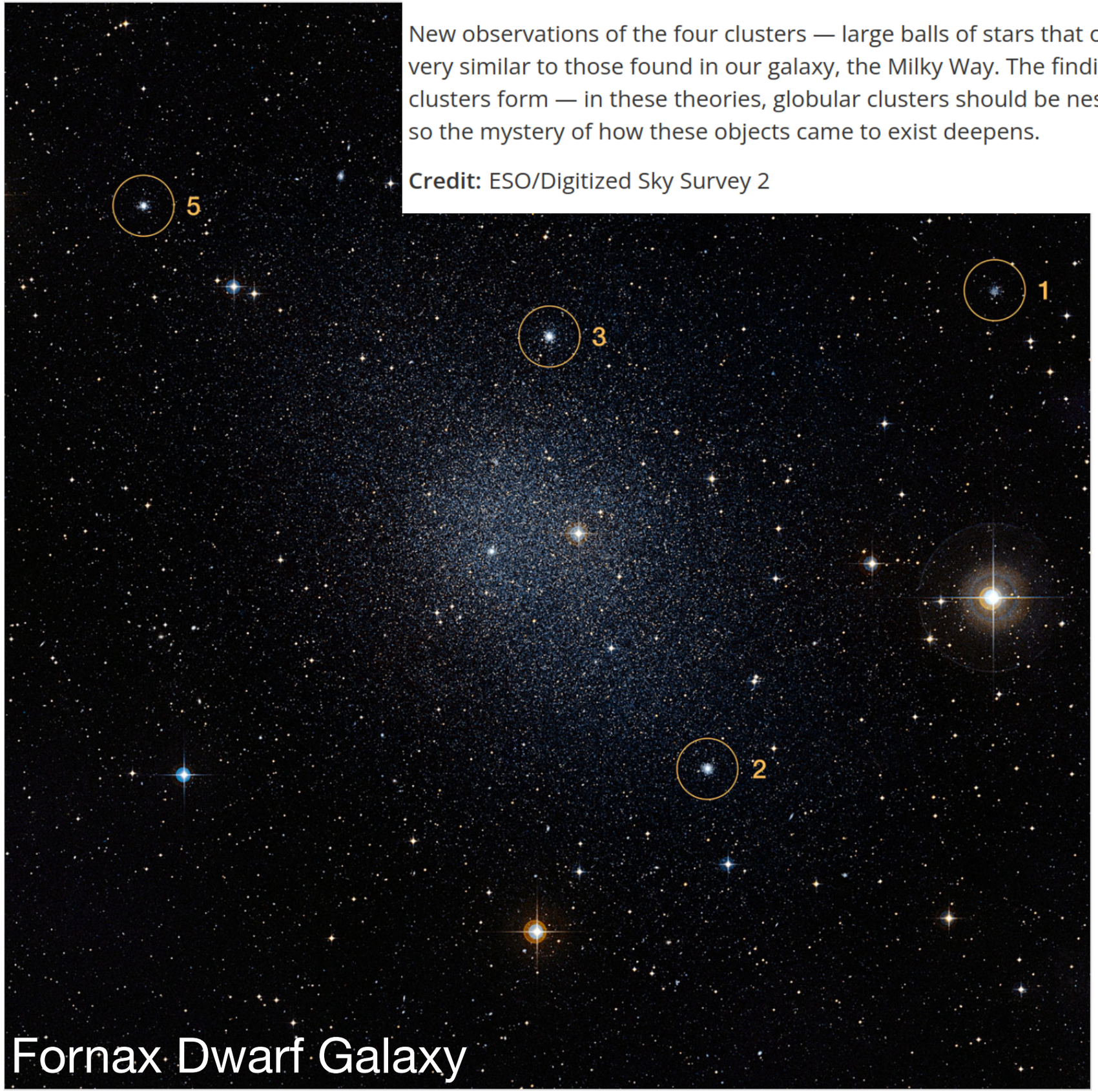

Monthly Notices
of the
ROYAL ASTRONOMICAL SOCIETY

MNRAS **457,** 479–486 (2016) doi:10.1093/mnras/stv2944

Limits on the significant mass-loss scenario based on the globular clusters of the Fornax dwarf spheroidal galaxy

P. Khalaj★ and H. Baumgardt★

School of Mathematics and Physics, University of Queensland, St. Lucia, QLD 4072, Australia

Accepted 2015 December 14. Received 2015 December 4; in original form 2015 November 12

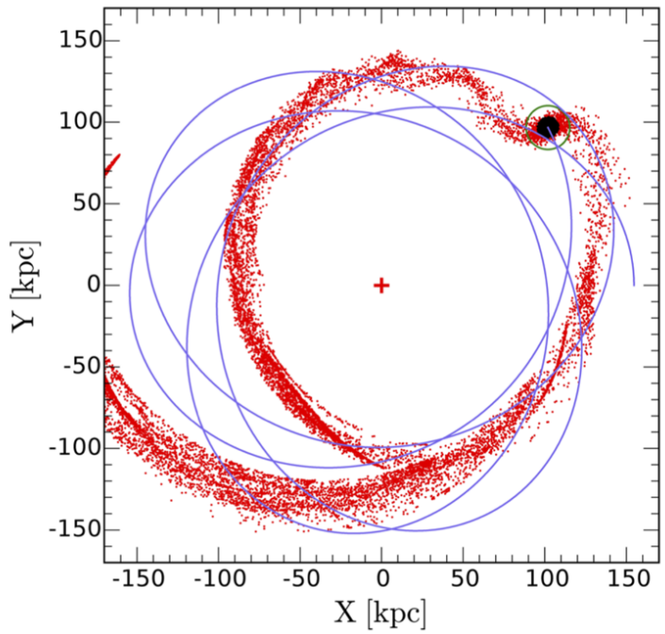

Figure 2. Spatial distribution of stars in the halo of the Milky Way for the LC model after one Hubble time. The Milky Way is denoted by the central cross at the origin. In this simulation, the initial distance of the stars from the centre of Fornax is $R = 3.0$ kpc and their initial speed is $v = 35\,\mathrm{km\,s^{-1}}$. Red points represent stars that have left Fornax (about 70 per cent mass loss). The clump of black points enclosed by the green circle shows stars that still reside within the tidal radius of Fornax. The radius of the green circle is equal to two times the tidal radius of Fornax at perigalacticon. The Rosette-like orbit of Fornax is shown by the blue solid line. In this figure, X and Y correspond to the coordinates of stars in the orbital plane of Fornax and not the Galactocentric rest frame defined in Section 2.1.

ABSTRACT

Many of the scenarios proposed to explain the origin of chemically peculiar stars in globular clusters (GCs) require significant mass loss (≥95 per cent) to explain the observed fraction of such stars. In the GCs of the Fornax dwarf galaxy, significant mass loss could be a problem. Larsen et al. showed that there is a large ratio of GCs to metal-poor field stars in Fornax and about 20–25 per cent of all the stars with [Fe/H] < -2 belong to the four metal-poor GCs. This imposes an upper limit of ∼80 per cent mass loss that could have happened in Fornax GCs. In this paper, we propose a solution to this problem by suggesting that stars can leave the Fornax galaxy. We use a series of N-body simulations to determine the limit of mass loss from Fornax as a function of the initial orbital radii of GCs and the speed with which stars leave Fornax GCs. We consider a set of cored and cuspy density profiles for Fornax. Our results show that with a cuspy model for Fornax, the fraction of stars that leave the galaxy can be as high as ∼90 per cent, when the initial orbital radii of GCs are $R = 2$–3 kpc and the initial speed of stars is $v > 20\,\mathrm{km\,s^{-1}}$. We show that such large velocities can be achieved by mass loss induced by gas expulsion but not mass loss induced by stellar evolution. Our results imply that one cannot interpret the metallicity distribution of Fornax field stars as evidence against significant mass loss in Fornax GCs, if mass loss is due to gas expulsion.

Assumed a smooth potential field for Dwarf Satellite (DSG)
- > N-body model is simplified to a three body model problem with MW, DSG and a GC

Assumptions

- DSG composed of N stars and a number of GCs with initial random conditions but in equilibrium
- DSG are collisionless systems -> smooth potential
- solution of the problem simplified to treatment of three bodies
- MW at the centre of a right-handed Cartesian coordinate system, with X-axis pointing towards the location of the Sun, Y -axis is in the direction of the Galaxy's rotation, Z-axis determined by the right-hand rule
- MW remains still throughout the simulation owing to its large mass.
- trajectory of the DSG is only determined by the MW
- GCs treated as point masses whose motion is prescribed by both the MW and the DSG.
- GCs are spatially distributed according to the density profile of their host DSG
- Initial velocities of GCs are drawn from a three-dimensional Maxwell-Boltzmann distribution.

2.1 Models

2.1.1 *The potential field of the MW*

For the MW, we adopt the well-known `MWPotential2014` model, described in Bovy (2015). In this model, the MW potential field consists of three components, namely bulge, disc, and halo. The bulge density follows a power-law distribution (spherical) with an exponential cutoff given by

$$\rho(r) \propto \frac{1}{r^{\alpha}} \exp\left(-\left(\frac{r}{r_{\rm c}}\right)^2\right) \tag{1}$$

The disc is a Miyamoto & Nagai (1975) model

$$\phi_{\rm disc} = \frac{-GM_{\rm d}}{\sqrt{x^2 + y^2 + \left(a + \sqrt{b^2 + z^2}\right)^2}} \tag{2}$$

It also assumes a dark-matter halo with a Navarro–Frenk–White potential (NFW) from Navarro et al. (1997)

$$\phi_{\rm halo} = -\frac{GM_{\rm vir}}{r} \frac{\log\left(\frac{c\,r}{r_{\rm vir}} + 1\right)}{\log(c+1) - \frac{c}{c+1}} \tag{3}$$

Time invariant

(+ Time variant)

2.1.2 *The potential field of the Sgr*

We assume a Plummer (1911) model for the present-day potential of the Sgr as follows

$$\phi_{\rm Sgr}(r) = -\frac{GM_{\rm Sgr}}{\sqrt{r^2 + r_{\rm sc}^2}} \tag{7}$$

Time invariant

(+ Time variant)

2.1.3 *The time-dependent potential models of the Sgr and the corresponding orbits*

We get the present-day equatorial coordinates (α, δ), proper motions $(\mu_\alpha \cos\delta, \mu_\delta)$, the line-of-sight velocity ($V_{\rm LOS}$), and the heliocentric distance ($D_\odot$) of the Sgr from the *Gaia* DR2 (see Table 5). For each of the potential models adopted for the MW, i.e. dynamic and static models as defined in Section 2.1.1, we trace back the orbit of the Sgr for 8 Gyrs to obtain its initial conditions.

In total, we consider eight different models to obtain the orbit of the Sgr. These models are labeled as L1 to L4 (light) and H1 to H4 (heavy). The characteristics of these models are summarized in Table 2.

Models with a static potential for the MW and the Sgr are designated by L1 and H1. The models labeled as L2 and H2 are as same as L1/H1, except that the dynamical friction also enters the equations of motion. We apply the standard form of dynamical friction to the halo (e.g. Binney & Tremaine 2011)

$$F_{\rm DF} = -0.428 \frac{GM^2}{r^2} \ln(\Lambda), \tag{8}$$

where r is the distance of the DSG from the centre of the MW, M is the mass of the DSG, and $\ln(\Lambda) = 3$ is the Coulomb logarithm.

In the H3 and L3 models, the MW and the Sgr potentials are considered as being dynamic (see Section 2.1.1). In H4 and L4 models, the Sgr and MW potentials are dynamic and the effect of dynamical friction has been considered. Tidal stripping induced by the MW has reduced the total mass (dark + baryonic matter) of the Sgr over the past 8 Gyrs. We have quantified this effect using an N-body simulation, where the Sgr is made up of $N = 50,000$ equal-mass particles distributed according to the Plummer model. The particles do not undergo stellar evolution. The motion of each particle is determined by the combined potential of all other particles as well as the MW, using an 8th-order Runge-Kutta integrator. We

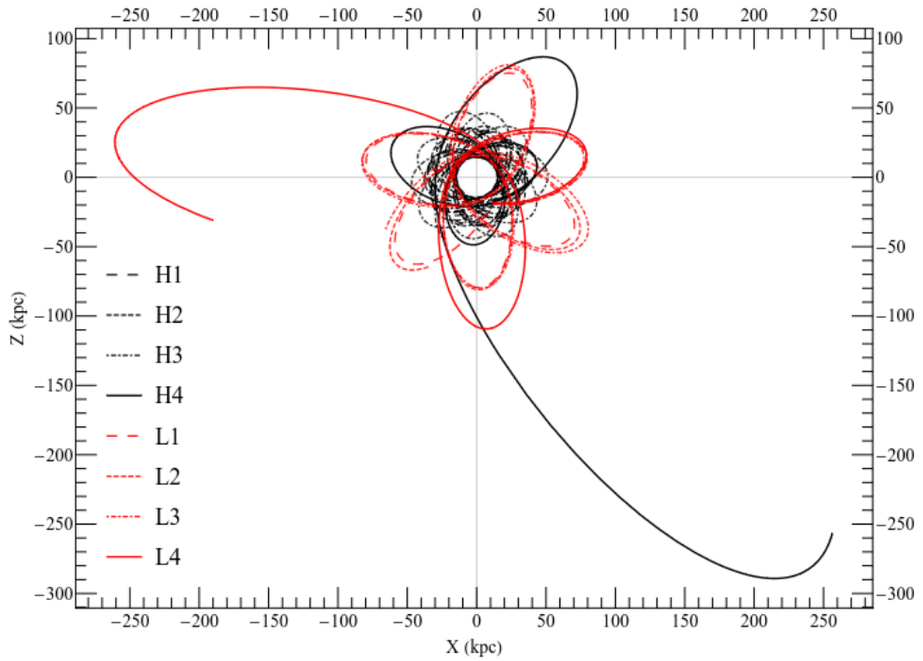

Figure 2. The orbit of the Sgr DSG in our eight simulation models for a period of 8 Gyrs. Orbits corresponding to light and heavy halo masses are shown in red and black, respectively. The orbits are depicted for the $X - Z$ plane of the Galactocentric coordinate.

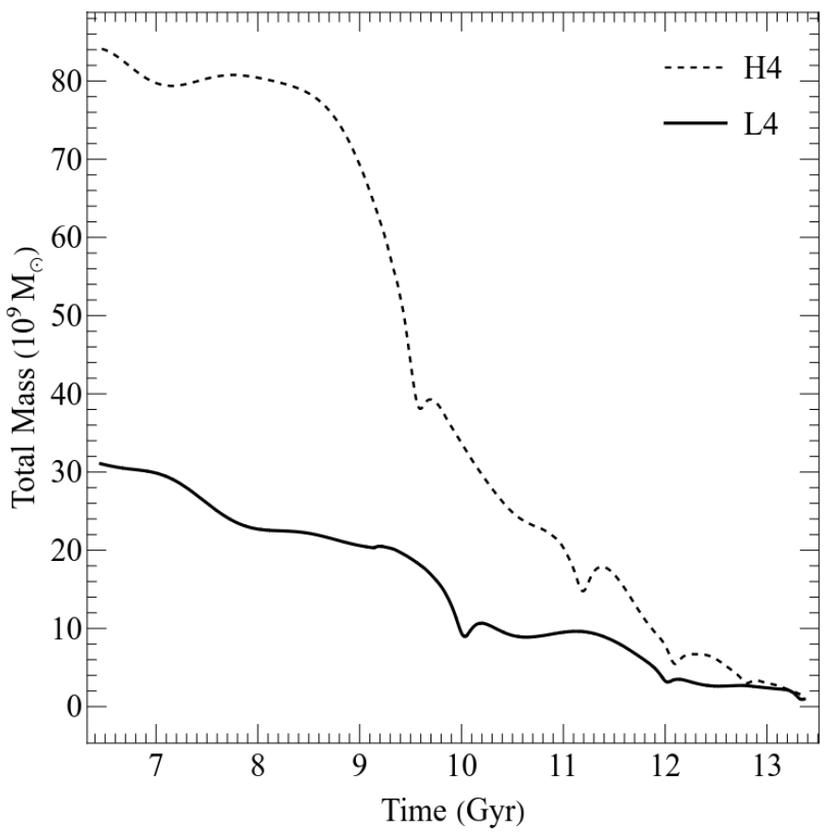

Figure 1. Time evolution of the Sgr total mass within the tidal radius in H4 and L4 models.

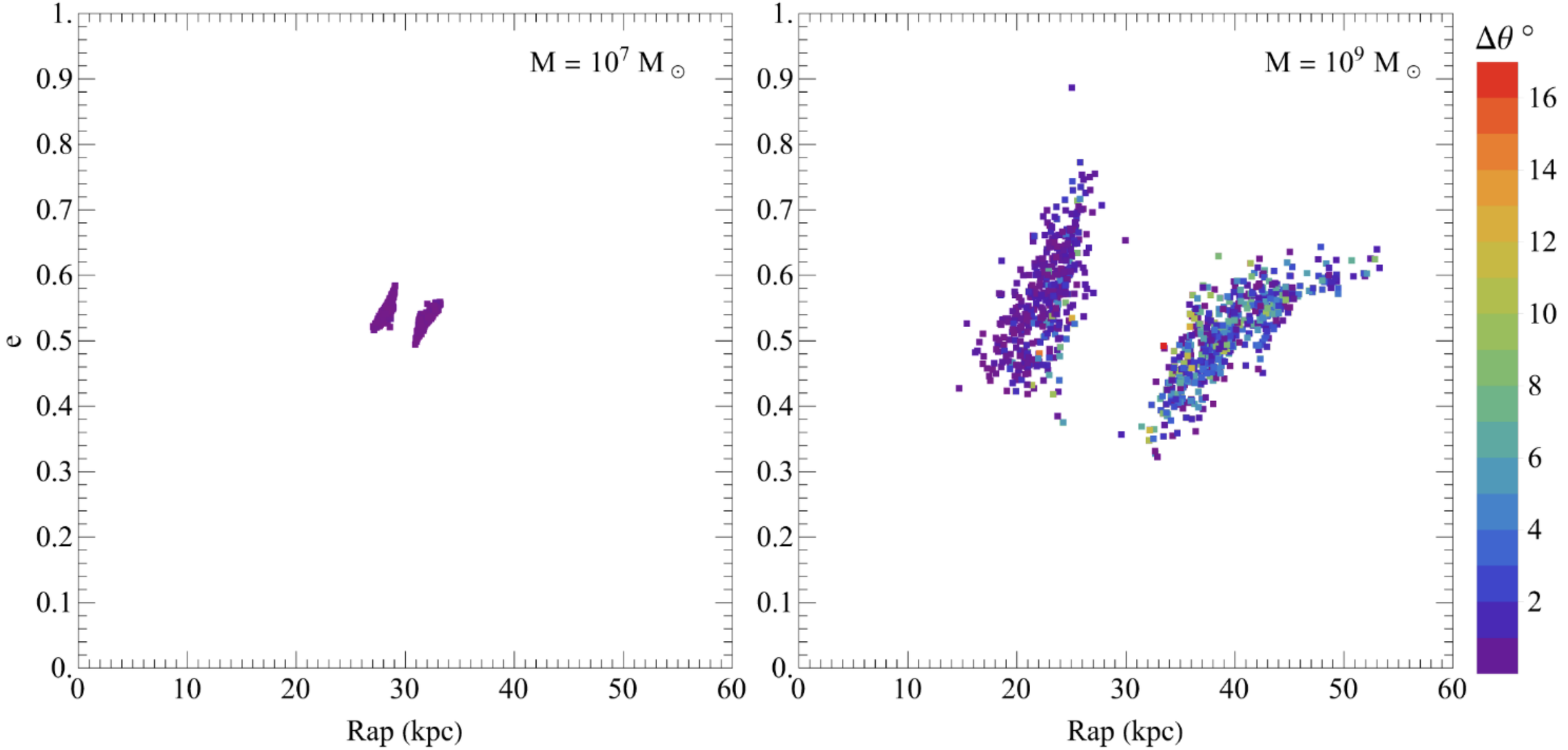

Figure 5. Orbital parameters of 1000 GCs escaped from two DSGs located on the MW disc after 8 Gyrs in the H1 model. The eccentricities of DSGs are 0.5. The colour coding represents the orbital inclination of GCs with respect to the DSG. The left and right panels correspond to DSG masses of 10^7 and 10^9 $M_\odot$, respectively.

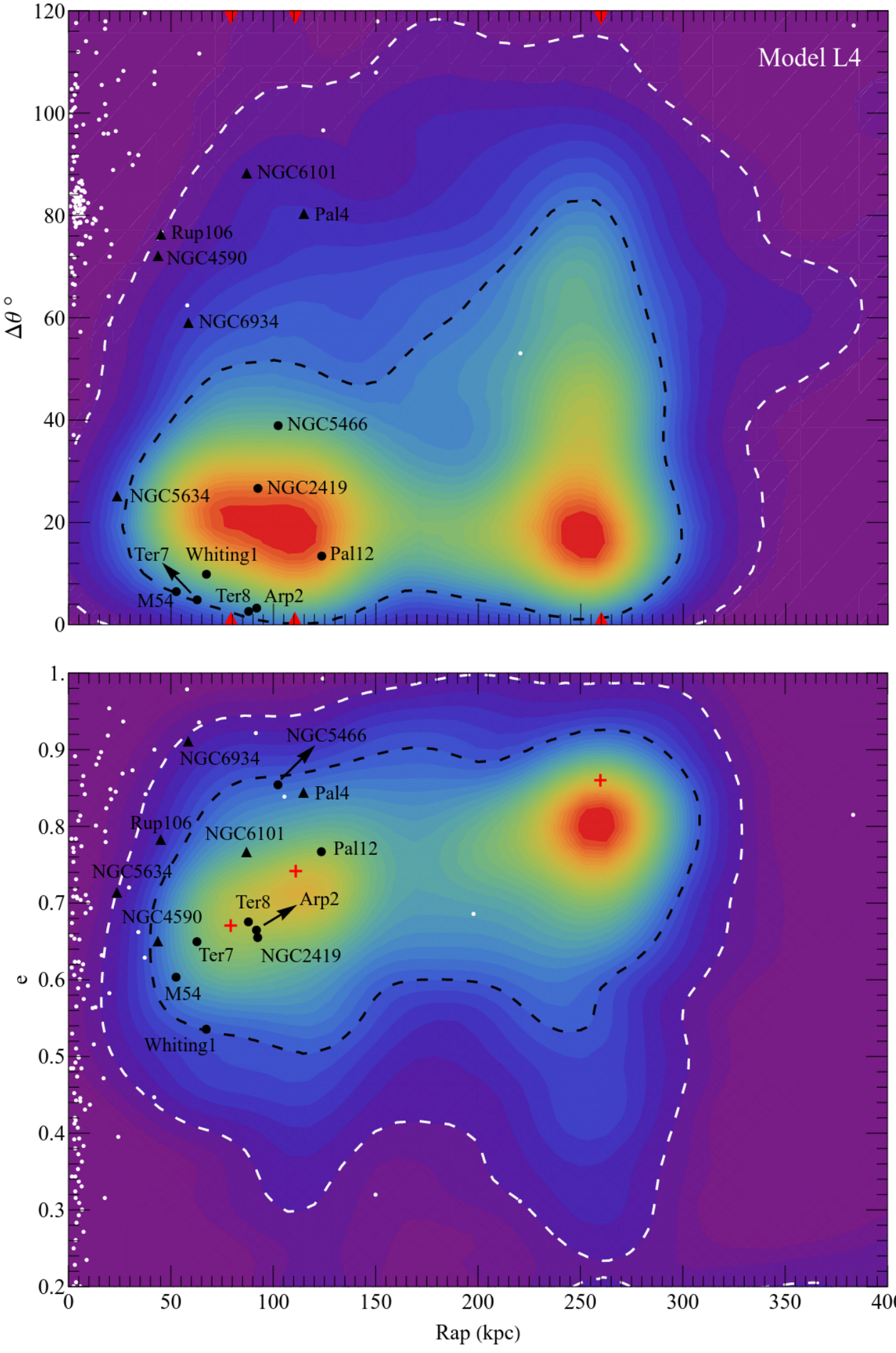

The scaled PDF of the Sgr runaway GCs, colour coded with respect to isodensity contours. The black and white contours correspond to boundaries enclosing 65%, and between 65% and 95% of all data, respectively. These provide the basis for categorizing the MW GCs into Flag 1 (black circles), Flag 2 (black triangles), and non-associations (white circles).

In the bottom panel, the red crosses mark the location of the Sgr in the parameter space as the Sgr spirals inwards as a result of dynamical friction. Likewise, the red arrow heads mark the apogalactic distances of the Sgr in the top panel, where we have $\Delta\theta = 0\circ$ for the Sgr. One can interpret non-associations as GCs with an association probability of less than 5%. The apparent placement of some points (e.g. non-associations) within the white or black contours is due to the fact that panels display projections. As a result, one needs to consider both panels together in order to infer the association categories.

The elongated peak on the left consists of two sub-peaks, i.e. there exists three peaks in unison with the ~3 apogalactic passages of the Sgr around the MW

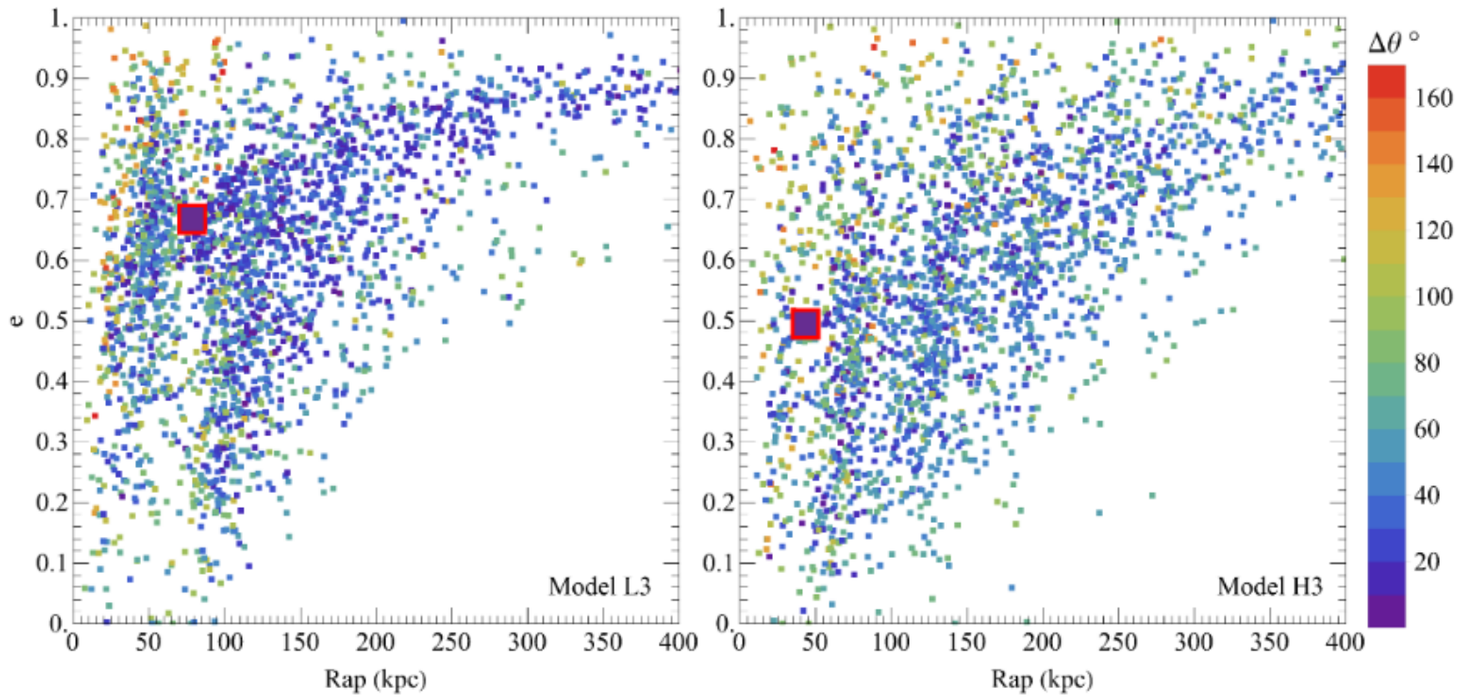

Figure 8. The orbital parameters of 2500 runaway GCs, from the Sgr in eight simulation models. The horizontal axis is the apogalactic distance (R_{ap}) in kpc and the vertical axis is the orbital eccentricity of these GCs. The colour coding corresponds to the orbital inclination of the GCs in degrees, with respect to the orbital plane of the Sgr. The large squares mark the Sgr. For models with dynamical friction, the position of the Sgr in the parameter space changes as a function of time. This has been shown by the magenta-filled square for the present day, and the white-filled squares for earlier epochs. For H2, H4, L2, and L4 models, the orbital parameters of the Sgr change over time as a result of dynamical friction.

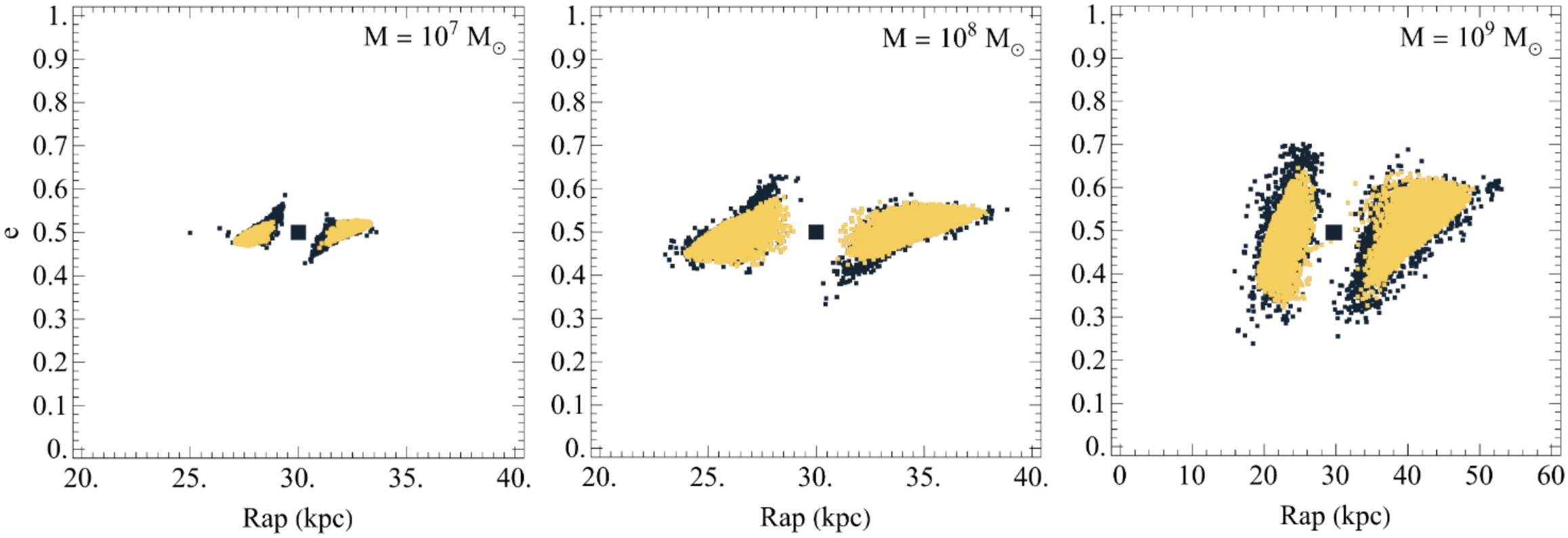

Figure 7. Distribution of R_{ap} and e of runaway particles from three DSGs located on the MW disc with orbital parameters of $R_{ap} = 30$ kpc and $e = 0.5$, obtained from NBODY6 (yellow) and our three-body method (black), for three DSG masses of 10^7, 10^8 and 10^9 $M_\odot$.

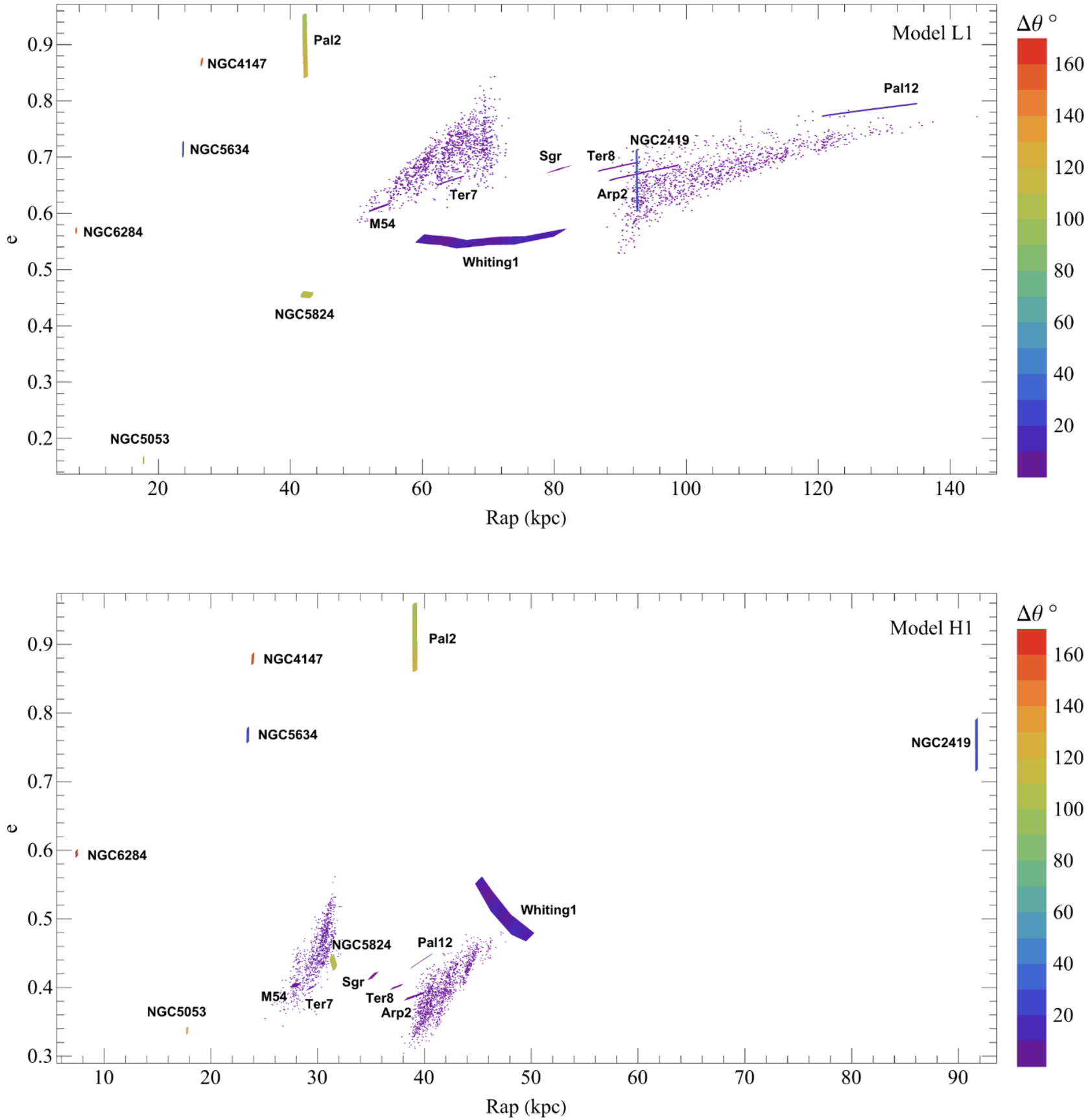

Figure 10. Orbital parameters of the Sgr runaway GCs (dots) and 13 MW GCs in L1 and H1 models, which have been previously suggested to be associated with the Sgr. The area occupied by each MW GC is due to its uncertainty of proper motions and the line-of-sight velocity. The Sgr is also depicted, considering the uncertainty of its observational data.

GC	H1	H2	H3	H4	L4	L3	L2	L1
NGC 6715 (M54)	1	1	1	1	1	1	1	1
Ter 7	1	1	1	1	1	1	1	1
Arp 2	1	1	1	1	1	1	1	1
Ter 8	1	1	1	1	1	1	1	1
Whiting 1	2	1	1	1	1	1	2	2
Pal 12	2	2	1	1	1	1	2	2
NGC 2419	-	-	1	1	1	1	2	2
NGC 5466	-	-	1	1	1	2	2	2
NGC 5634	-	-	2	1	2	1	-	-
NGC 4590	-	-	1	2	2	1	-	-
Rup 106	-	-	2	2	2	1	-	-
Pal 4	-	-	1	2	2	2	-	-
NGC 6101	-	-	1	-	2	2	-	-
NGC 5897	-	-	2	2	-	2	-	-
NGC 6235	-	-	2	2	-	2	-	-
NGC 6934	-	-	-	-	2	2	-	-
NGC 6426	-	-	2	2	-	-	-	-
IC 4499	-	-	2	-	-	2	-	-

Table 3. List of GCs that could be associated with the Sgr in all simulation models. The numbers indicate the association flags. Flag 1 GCs have the highest probability of being associated with the Sgr (ref. Section 2.2.1).

Conclusions

- comparison between the results of three-body method and that of the NBODY6 code exhibits the same distribution of runaway particles in the orbital parameter space

- the distribution of runaway GCs is not random and does not cover the entire parameter space. Rather, it exhibits a dichotomous pattern. In particular, the runaway GCs form two distinctive populations, a population in which $R_{\rm ap}$ (GC) $<R_{\rm ap}$ (DSG) and another one with $R_{\rm ap}$ (GC) $> R_{\rm ap}$ (DSG)

- positive correlation between the mass of a DSG and the dispersion of its runaway GCs in the parameter space

- DSGs that are close to massive DSGs such as the Sgr or the LMC, the orbital parameters of runaway GCs can be significantly perturbed by the massive DSG, to the extent that, some of the GCs might be even recaptured by the massive DSG

- identified 18 GCs which are associated with the Sgr

- in total, identified 29 MW GCs which could have originate from DSGs, indicating a maximum of 19% of all MW GCs could have an ex-situ origin